Estuaries and Coasts
https://doi.org/10.1007/s12237-021-00959-6

Estimating the Influence of Oyster Reef Chains on Freshwater Detention at the Estuary Scale Using Landsat-8 Imagery

Alice Alonso[1,2] · Natalie G. Nelson[1,3] · Simeon Yurek[4] · David Kaplan[5] · Maitane Olabarrieta[6] · Peter Frederick[7]

Received: 30 October 2020 / Revised: 26 February 2021 / Accepted: 17 May 2021

Abstract

Oyster reef chains grow in response to local hydrodynamics and can redirect flows, particularly when reef chains grow perpendicular to freshwater flow paths. Singularly, oyster reef chains can act as porous dams that may facilitate nearshore accumulation of fresh or low-salinity water, in turn creating intermediate salinities that support oyster growth and estuarine conditions. However, oyster-driven freshwater detention has only been confirmed by limited, point-scale observational data, and simplified models. Oyster reef-driven freshwater detention in real ecosystems at the estuary scale remains largely unexplored. In this study, we analyzed the visible bands in 30-m resolution remote sensing (RS) images recorded by the Operational Land Imager aboard Landsat-8 to characterize the freshwater detention effect of oyster reef chains across a set of hydrologic conditions. Our results support prior findings indicating that 30-m resolution RS images recorded by the Operational Land Imager aboard Landsat-8 are useful for analyzing coastal dynamics after atmospheric correction, despite having been originally designed for terrestrial studies. Statistical models of water-leaving reflectance revealed that freshwater detention by oyster reefs was evident across the estuary, with the greatest effect occurring in the region closest to shore. Additionally, statistical modeling results and spatial patterns apparent in the satellite images suggested that reef-driven freshwater detention occurred under high riverine discharge conditions, but was less evident when flow was low. Beyond offering insight on the potential role of oyster reefs as mediators of estuarine hydrology, this study presents a transferable methodological framework for exploring estuarine biophysical feedbacks in black-water river estuaries using satellite remote sensing.

Keywords Landsat 8 · Satellite imagery · Salinity · Oyster reefs · Suwannee River · Gulf of Mexico

Introduction

Global estimates indicate that 85% of the world's oyster populations are in decline or already lost (Beck et al. 2011). These declines are largely attributed to overharvest, disease, parasitism, dredging and trawling, competition from exotic species, water quality degradation, and combinations thereof (NOAA Fisheries Eastern Oyster Biological Review Team 2007). The loss of oysters is concerning not only with regard to their economic, social, and cultural values, but also their value to ecosystems. Oysters and the reefs they construct provide many ecosystem services, from serving as sheltering and

Communicated by Richard C. Zimmerman

✉ Natalie G. Nelson
nnelson4@ncsu.edu

[1] Biological and Agricultural Engineering, North Carolina State University, Raleigh, NC, USA

[2] Earth and Life Institute, Université catholique de Louvain, Louvain-la-Neuve, Belgium

[3] Center for Geospatial Analytics, North Carolina State University, Campus Box 7625, Raleigh, NC 27695, USA

[4] U.S. Geological Survey, Wetland and Aquatic Research Center, Gainesville, FL, USA

[5] Environmental Engineering Sciences, Engineering School of Sustainable Infrastructure & Environment, University of Florida, Gainesville, FL, USA

[6] Civil and Coastal Engineering, Engineering School of Sustainable Infrastructure & Environment, University of Florida, Gainesville, FL, USA

[7] Wildlife Ecology and Conservation, University of Florida, Gainesville, FL, USA

Published online: 26 May 2021

foraging habitat for a wide variety of species, to filtering the water column, sequestering nutrients and particulates, and stabilizing nearshore and intertidal habitats, among other services (Grabowski and Peterson 2007; Scyphers et al. 2011; Grabowski et al. 2012). Ecosystem services provided by oyster reefs are valued at $5500 to $99,000 USD per hectare per year (Grabowski et al. 2012).

Reefs take on different morphologies depending on local hydrodynamics, from irregular "patch" reefs that form away from shore, to "fringe" reefs that line tidal creek banks (Kennedy and Sanford 1999; Colden et al. 2016). In estuaries with fast flows and shallow and relatively uniform bathymetry, linear "string" reefs form. String reefs often grow perpendicularly to freshwater flow paths as they interact with, and mediate, local hydrology (Kennedy and Sanford 1999). Researchers have offered several potential explanations as to how morphologically diverse reef structures form in response to different hydrodynamic regimes, and how different reef geomorphologies benefit oyster populations (Walles et al. 2015). A general hypothesis is that local improvements in habitat conditions are created through interactions between hydrology and reef geomorphology, for example, through enhanced feeding potential for oysters and decreased occurrence of deleterious effects such as sediment deposition, hypoxia, and aerial exposure (Kennedy and Sanford 1999; Lenihan 1999; Colden et al. 2017). Such feedbacks are believed to explain non-random spatial patterning of biogenic reefs and reef patches at the estuary scale, which has been observed in estuaries with oyster reef complexes (Hedgpeth 1953; Haven and Whitcomb 1983; M. G. McCormick-Ray 1998; J. McCormick-Ray 2005). These patterns are also observed, and particularly well studied, in mussel beds. Mussel beds form linear structures perpendicular to the dominant direction of flow in estuaries with strong tidal currents, whereas this banded spatial structure is not evident in systems with slow-moving currents (Ysebaert et al. 2009; van de Koppel et al. 2012). The banded spatial configuration of mussel beds is believed to occur due to a combination of local interactions and physical forcing at the estuary scale (Rietkerk and van de Koppel 2008; van de Koppel et al. 2012). Specifically, waters that flow directly over mussel beds become depleted of phytoplankton as the mussels filter feed from the water column, creating competition for food in the areas adjacent to the bed (van de Koppel et al. 2005). Strong tidal currents deliver and replenish phytoplankton stocks, in turn minimizing resource depletion along the dominant direction of flow (van de Koppel et al. 2012) and, hence, supporting the development of the mussel beds. Such effects are also likely to contribute to the patterns observed in other biogenic structures, such as oyster reefs.

As yet another hypothesis as to how hydrodynamics may influence the spatial configuration of reefs, Kaplan et al. (2016) proposed that formation of shore-parallel reefs in riverine estuaries contributes to regulation of coastal salinity regimes, which can be highly beneficial for oyster reef communities. Intermediate ranges of salinity, e.g., 14–28 ppt, are generally considered optimal for the Eastern oyster, *Crassostrea virginica* (Petes et al. 2012; Havens 2015; Lowe et al. 2017). Outside of this range, oysters still survive and persist, but are increasingly subject to predation, parasitism, and disease on the high end of salinity (Aguilar Marshall et al. 2019), and increased mortality on the low end, particularly when water temperatures are high (Rybovich et al. 2016). Thus, maintenance of intermediate salinity ranges is generally considered critical for supporting long-term persistence of oyster reefs (Petes et al. 2012; Lowe et al. 2017), and the oysters themselves may play a role in maintaining these regimes. By forming linear reefs perpendicular to dominant freshwater flows discharging from the coast, oyster reefs in aggregate may act as porous dams that facilitate nearshore detention of freshwater, thereby creating a positive feedback by which oysters engineer the surrounding water quality to support their own growth (Kaplan et al. 2016).

The ability of reefs to detain freshwater has been evidenced by *in situ*, high-frequency salinity measurements, which revealed a salinity differential across the land- and seaward sides of a reef located in the northeastern Gulf of Mexico (Kaplan et al. 2016). The same study proposed the potential for oyster reefs to regulate salinity over extensive estuarine areas, as confirmed through hydrodynamic modeling. However, the modeling approach was largely conceptual and used simplified estuarine bathymetry, assumed constant river discharge, simulated tides, and neglected wind forcing. Empirical evidence of oyster-driven freshwater detention at large geographic scales (i.e., entire estuary, regional) and under real-world conditions has not yet been produced. Questions also remain about the capacity for reef complexes, i.e., multiple oyster reefs, to affect freshwater detention across an estuary. Resolving estuary scale effects of reef-driven freshwater detention with empirical evidence would require extensive salinity and flow data across space and time, making the prospect of directly observing reef-freshwater feedbacks costly and time consuming. Alternatively, satellite remote sensing offers a cost-effective approach to observing freshwater accumulation and dispersion across time and space in relation to oyster reefs, which we propose is especially possible in estuaries that receive discharge from blackwater rivers.

"Blackwater" rivers typically drain wetland-dense landscapes and consequently have high concentrations of colored dissolved organic matter (CDOM), which strongly absorbs short wavelength light and gives blackwaters their characteristic black-brown color (Robinson 1983; Bowling et al. 1986; Carder et al. 1989; Nichol 1993a; Paavel et al. 2011; Kutser et al. 2016; Cao et al. 2018). Blackwater rivers are found throughout the world in regions with organic-rich soils and low elevation gradients, such as boreal peatlands and tropical

rainforests, and are particularly common in the southeastern USA (Meyer 1990). CDOM-rich blackwater river discharge starkly contrasts with the characteristically blue-green waters of marine systems, making color a proxy for freshwater presence and salinity in blackwater-fed estuaries. Correlations between CDOM and salinity are well-documented for many estuarine systems (Ferrari and Dowell 1998; Bowers and Brett 2008; Chaichi Tehrani et al. 2013; Chaichitehrani et al. 2014; Cao et al. 2018). Evidence of relationships between CDOM and salinity provide support for the assumption that color, which is readily detectable via satellite sensors, can be used as a proxy spectral signature for freshwater in these systems. Several studies have leveraged the contrast in reflectance spectra between fresh and marine waters to track the dispersal of river plumes in coastal waters from satellite imagery (Vasilkov et al. 1999; Devlin et al. 2015; Constantin et al. 2016; Le et al. 2016; Rudorff et al. 2018), demonstrating how satellite remote sensing could be used to explore the effect of oyster reefs on freshwater detention at the estuary scale by evaluating how water color, i.e., freshwater, varies in relation to oyster reef locations.

Although satellite sensors offer compelling opportunities for nearshore monitoring, nearshore satellite remote sensing analyses must contend with several limitations and challenges inherent to optical imagery of the coastal zone. Heritage products from satellite missions designed for ocean color survey have coarse pixel sizes that limit their utility for nearshore analyses; for example, the widely used products from the Medium Resolution Imaging Spectrometer (MERIS), Moderate Resolution Imaging Spectroradiometer (MODIS; NASA n.d.), Ocean and Land Color Instrument (OLCI) aboard Copernicus Sentinel-3 (Drusch et al. 2012), and Sea-Viewing Wide Field-of-View Sensor (SeaWIFS; NASA 2014) images have spatial resolutions ranging between 250 and 9000 m. Finer-resolution optical satellite products, primarily developed for land use and land cover studies, are characterized by lower digital resolution and larger bandwidths. As a result, observations collected from finer resolution sensors have low signal-to-noise ratios, making the observations largely unsuited for aquatic system analysis due to the weak water-leaving reflectance accounting for less than 10–20% of the total signal in the visible spectrum measured by the satellite sensor (Gordon 1978; Robinson 1983; Warren et al. 2019). The remaining 80–90% of the signal from the visible spectrum is attributed to sunlight that is scattered and absorbed through interactions with aerosols and molecules in the atmosphere; these effects are removed through a process called "atmospheric correction." Furthermore, shallow nearshore environments have complex water-leaving spectral reflectance signatures composed of reflectance from the seafloor (referred to as "bottom reflectance") and the water column (Maritorena et al. 1994; Zhao et al. 2013; Li and Roy 2017), which complicate satellite remote sensing analyses of coastal waters.

A number of recent studies have demonstrated that the enhanced capabilities of the Operational Land Imager (OLI) aboard Landsat-8 (launched in 2013) produce observations reliable for investigating inland and nearshore waters (Franz et al. 2015; Pahlevan et al. 2017a, 2017b; Wei et al. 2018). Landsat-8 is a near-polar orbiting satellite that records images over a 185 km swath at a spatial resolution of 30 m, and with a revisit time of approximately 16 days. In comparison to previous Landsat sensors, OLI also has increased digital resolution and radiometric performance with an improved signal-to-noise ratio, allowing for better detection and differentiation of water-leaving reflectance. The bandwidth has also been narrowed in comparison to the heritage Landsat products and an additional band is measured in the blue region of the spectrum, referred to as the "deep blue" band (wavelength = 430–450 nm), in order to facilitate coastal and aerosol studies. Because of these improved properties, studies have shown that Landsat-8 images allow for finer scale monitoring of coastal processes and create new opportunities to understand spatial patterns and temporal dynamics of coastal and ecological processes.

This study sought to address knowledge gaps surrounding the role of oyster reef chains as mediators of estuary-scale freshwater detention by analyzing spatial variation in water color across an estuary with two large, shore-parallel reef chains using Landsat-8 imagery. Our central hypothesis was that shore-parallel reef chains detain freshwater in the nearshore at the estuary scale (> 10 km^2). We assumed that, if oyster reef chains detained freshwater at the estuary scale, CDOM-rich blackwaters would accumulate on the landward sides of the reefs, creating spatial patterns in water color that were coincident with the locations of the reef chains and discernable through Landsat-8 imagery. The influence of oyster reef chains on freshwater regulation under different hydrologic conditions (i.e., low vs. high freshwater river inflows) was characterized through statistical modeling of estuarine water reflectance across transects that started from the shore, spanned two reef chains, and ended in open marine waters. In addition to providing new insights on relationships between oyster reef complexes and freshwater detention at the estuary scale, the methods applied here can be used more generally as a framework for using satellite remote sensing to evaluate a range of biophysical processes in blackwater river-fed estuaries.

Methods

Site Description

Our study focused on the Suwanee River estuary, also referred to as the Suwanee Sound, which is the same system analyzed in the study that first proposed how oyster reefs serve as

porous dams in estuaries (Kaplan et al. 2016). The Suwannee River originates in the Okefenokee Swamp in Georgia (USA), receives inputs from the Alapaha, Withlacoochee, and Santa Fe Rivers, flows southwest through a karstic basin, and discharges to the Gulf of Mexico in Florida's Big Bend to form the Suwannee Sound (Fig. 1). The Suwannee River discharges to the Suwannee Sound trough two main channels: the "West Pass" and the "East Pass" (Fig. 1; Bales et al. 2006). The Suwanee Sound is home to a large Eastern oyster (*Crassostrea virginica*) reef complex that consists of several shore-parallel string reef chains, including the Half Moon Reef, Lone Cabbage Reef, and the Great Suwanee Reef. The Lone Cabbage Reef was the focus of the Kaplan et al. (2016) study. Each of these "reefs" in the Suwannee Sound actually consists of several string reef segments that form chains. Thus, when referring to specific reef structures like the "Lone Cabbage Reef" or "Great Suwannee Reef," we are referring to the reef chains composed of many individual reef segments. Lone Cabbage (inshore) and Great Suwannee (offshore) Reefs both consist of reef chains that are parallel to the shoreline and in series relative to freshwater flow, making these reefs ideal for investigating interactive and estuary-scale relationships between oyster reefs and freshwater detention. Lone Cabbage Reef is 5.2 km in length, with approximately 23 segments ranging from 30 to 280 m in length and approximately 20–40 m in width. The Great Suwannee Reef is approximately 10 km in total length, but the lengths of individual

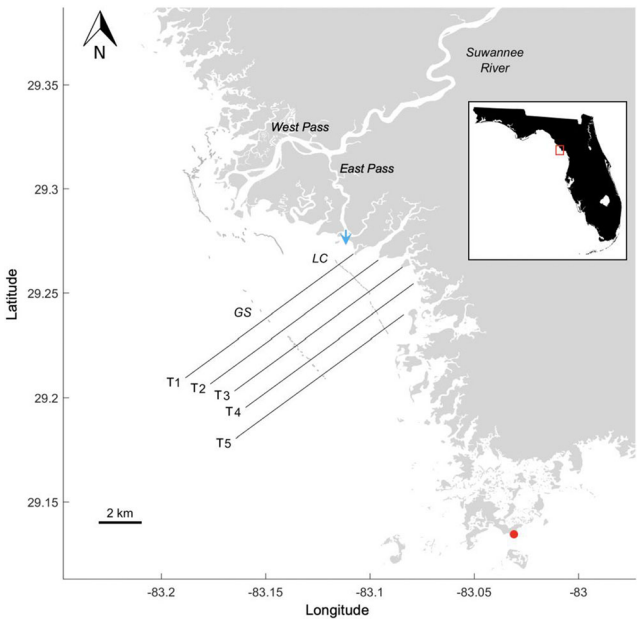

Fig. 1 The Lone Cabbage (LC) and the Great Suwannee (GS) Reefs in the Suwannee Sound, and the five transects considered in the study (T1 to T5). The inset map shows the location of the study area on the Gulf Coast of Florida, USA. The blue arrow shows where the East Pass of the Suwannee River discharges to the coast. The red circle (bottom-right) corresponds to the location of the nearest sea level gauge, located at Cedar Key (U.S. NOAA Tides and Currents station ID 8727520)

segments are difficult to measure because they are so degraded. The average of the tops of 28 nearby natural reefs (within 10 km, mostly inshore of the Lone Cabbage Reef) was −0.442 m elevation (North American Vertical Datum) and 0.245 m above mean low low water (MLLW) at the Cedar Key tide gage (Fig. 1) (Frederick 2021).

Although many reefs exist within the Suwannee Sound, their modern condition is severely degraded, with loss of shell coverage and rapid decrease in elevation. Loss of live shell coverage is proposed to result from long-term reductions in freshwater flows to the estuary, resulting in episodic periods of high salinities and consequent mortality events (Seavey et al. 2011). Kaplan et al. (2016) hypothesized a positive feedback at the ecosystem level: as shell coverage is reduced, reefs become less able to recruit young oysters, the rugosity of the reefs reduces, and the surface elevation erodes, presumably reducing the ability of the reef chain to detain fresh or brackish water, further reducing suitability for recruitment and retention by oysters. This cycle is thought to be self-reinforcing, and, at some point, the reefs become locked into an alternative state that is unable to maintain oyster coverage (Jordan-Cooley et al. 2011; Colden et al. 2017). Understanding the reef-freshwater relationships in this estuary is thus particularly relevant, especially in light of ongoing large-scale efforts to restore the Lone Cabbage Reef (Pine et al., unpublished) and other reefs like it (Bersoza Hernández et al. 2018).

Mean daily discharge in the lower Suwannee River is approximately 280 ± 190 m^3 s^{-1}, and generally peaks from February to April (Farrell et al. 2005). The Suwannee's wetland origins contribute large amounts of dissolved organic carbon (DOC) to the water, resulting in dark black-brown waters with color above 350 platinum-cobalt units (PCU) in upstream reaches (Farrell et al. 2005). Several first magnitude, clear-water springs discharge to the Lower Suwannee River (Katz et al. 1997; Farrell et al. 2005), reducing the river's color in downstream reaches. Despite the influence of spring flows, water color throughout the Suwannee River remains high even in periods of lower discharge, with water color in its coastal plume ranging from approximately 101–125 PCU in the nearshore environment to 26–75 PCU along the seaward fringes of the plume (Bledsoe and Phlips 2000).

Remote Sensing and Analysis of Water Color

The analysis presented here leverages the relationship between water color and water source (i.e., blackwater of the Suwannee River vs. blue-green water from the Gulf of Mexico) to estimate spatial trends in freshwater composition and, hence, freshwater detention across the Suwannee Sound. Given that CDOM strongly absorbs short wavelength light, we assume that freshwater detention corresponds to decreases in water-leaving reflectance in the blue-green range of the visible electromagnetic spectrum (Fig. 2).

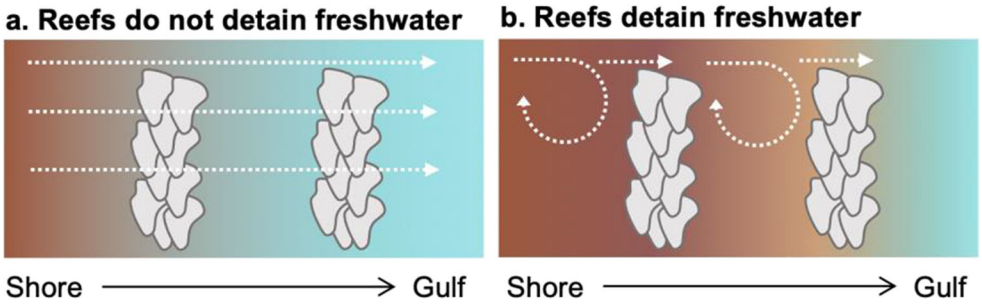

Fig. 2 Illustration of the conceptual representation of the study hypothesis. **a** We assume that, if the reefs do not affect freshwater detention, the freshwater reflectance signal decreases gradually as a function of distance from the shore. **b** Conversely, if reef chains detain freshwater, we assume that darker waters will accumulate on the landward sides of the reefs, which would result in lower water-leaving reflectance

Satellite Imagery

For this study, we downloaded the Landsat Collection 1 Tier 1 Top of Atmosphere data from the U.S. Geological Survey (USGS) Earth Explorer (https://earthexplorer.usgs.gov). The images were processed with the Level 1 to Level 2 generator (l2gen) in the SeaWiFS Data Analysis System v.7.5.1 (SeaDAS; Baith et al. 2001) to correct for atmospheric components in the signal and to mask land features. We used the Landsat-8 default coefficient values for aerosol selection and vicarious gain as provided by Pahlevan et al. (2017a, 2017b).

Two Landsat-8 images were selected for this analysis (Fig. 3): one captured during a period of high freshwater discharge in the Suwannee Sound (20 FEB 2015), and another during a period of lower freshwater discharge (17 APR 2018) (Fig. 4). These two images were selected from the full Landsat-8 collection based on image quality (i.e., low cloud cover and absence of shadows) and acquisition times that occurred during distinct freshwater flow conditions and during low tide. Images captured at low tide were prioritized since the tidal energy would be exerting the least force against riverine outflows, thus maximizing the influence of freshwater

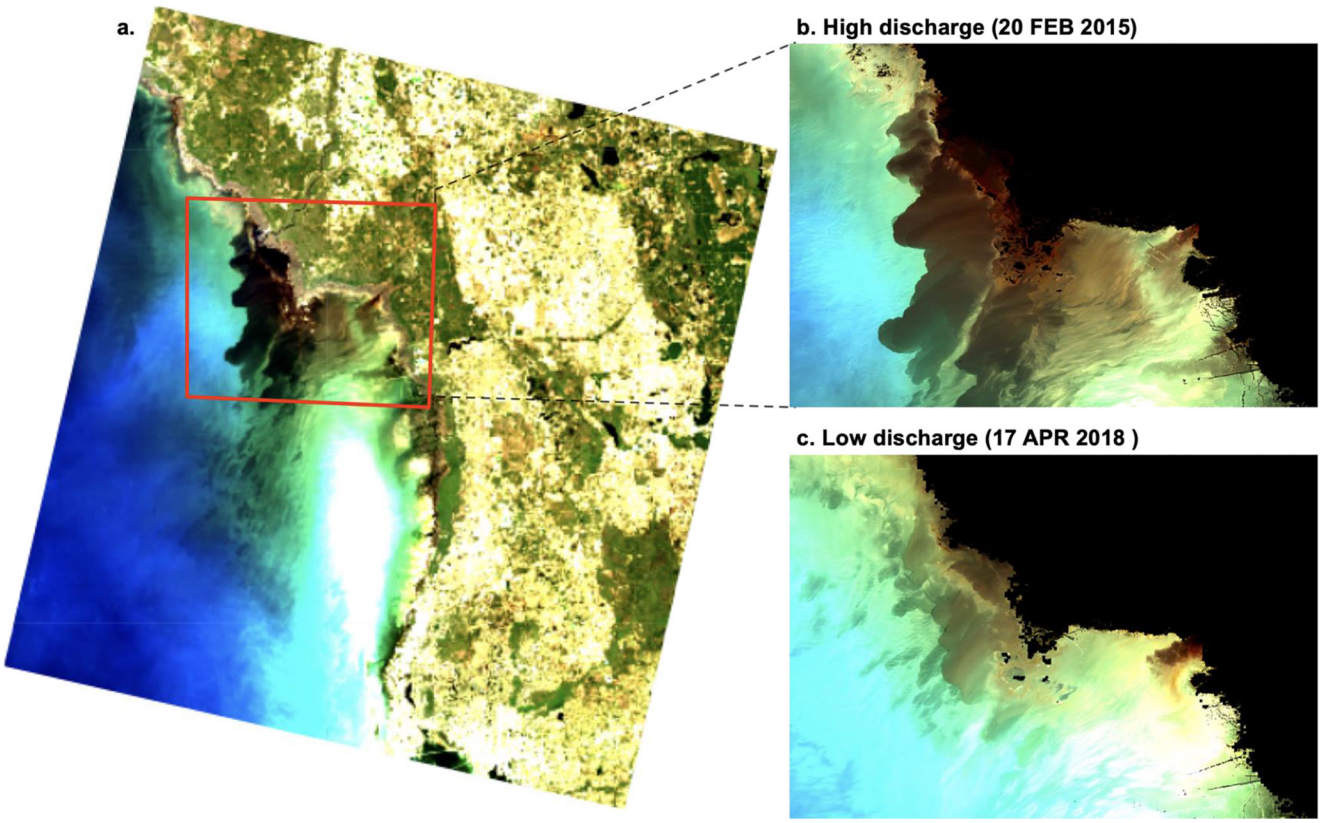

Fig. 3 **a** The full Landsat-8 tile shown in pseudo-true color, acquired on February 20, 2015 (20 FEB 2015). **b** Atmospherically corrected version of the image shown in (**a**), zoomed in to the study area. **c** Atmospherically-corrected Landsat-8 image acquired on April 17, 2018 (17 APR 2018), also zoomed into the study area. In (**b**) and (**c**), land and sand features have been masked out and are shown in black

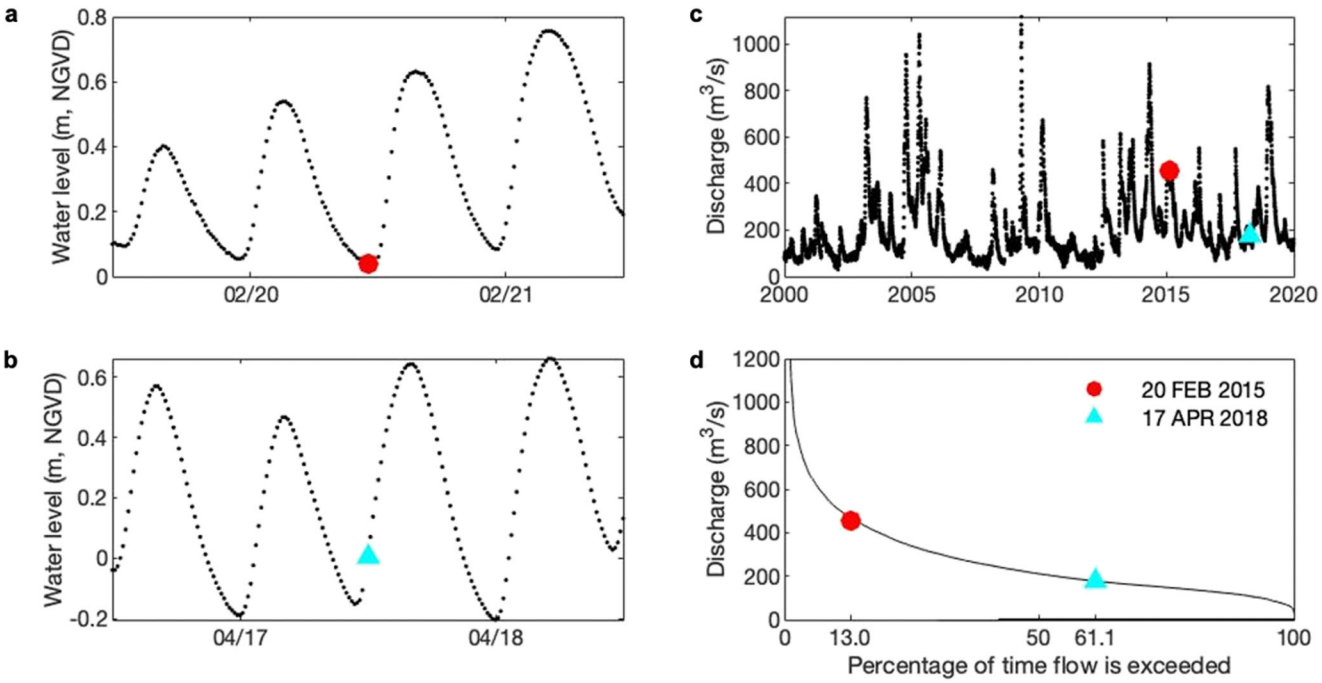

Fig. 4 Surface water level in the lower Suwannee River observed on **a** 20–21 of February 2015 (time of Landsat-8 image acquisition shown as a red point), and **b** 17–18 of April 2018 (time of image acquisition shown as a blue triangle). Suwannee River discharge **c** time series and **d** flow duration curve based on observations collected from 02/02/1951 to 12/31/2019, with the discharge at the times of image acquisition shown as a red point and blue triangle for the images captured on 20 February 2015 and 17 April 2018, respectively. Water level data were retrieved from USGS station 02323592; flow data were retrieved from USGS station 02323500

flow in the estuary and potential for detecting oyster reef-driven freshwater detention. The image corresponding to high freshwater discharge (20 FEB 2015) was acquired at low tide (Fig. 4a) when river discharge was approximately 456 m^3 s^{-1} (Fig. 4c), a rate exceeded only 13% of the time based on data collected from 1951 to 2019 (Fig. 4d). The image corresponding to lower freshwater discharge (17 APR 2018) was acquired shortly after low tide (Fig. 4b); at this time, river discharge was approximately 176 m^3 s^{-1} (Fig. 4c), a flow rate exceeded 61% of the time (Fig. 4d). Flow data were retrieved from USGS station 02323500 (Suwannee River near Wilcox); water level data were retrieved from USGS station 02323592 (Suwannee River at Gopher River). These images were collected roughly 3 years apart; however, this period is small compared to the time scale of the decline of LC Reef (several decades), and there were no major storm events in the interim. As far as we know, much of the degradation of the reef system occurred in preceding decades (Seavey et al. 2011); thus, we assume reef morphology or ecology does not vary between the time of acquisition of the two images, making the images comparable for our purposes.

Spectral Reflectance as a Proxy for Water Color

Waters with high levels of organic matter strongly absorb short wavelength light (Robinson 1983; Bowling et al. 1986; Carder et al. 1989; Nichol 1993a; Paavel et al. 2011; Kutser et al. 2016; Cao et al. 2018). In other words, spectral reflectance (R_{rs}) in the blue-green portion of the spectrum for blackwaters is particularly low relative to seawater (Robinson 1983; Nichol 1993a; Nichol 1993b). The blue-green region corresponds to band 1 (B1; 430–450 nm), band 2 (B2; 450–510 nm), and band 3 (B3; 530–590 nm) in Landsat-8 products. We looked at the spatial distribution of spectral reflectance in these bands as a proxy of water color and, hence, freshwater across the Suwannee Sound. We also paid specific attention to the spectral reflectance ratios between band 3 (561 nm, green) and band 4 (655 nm, red), i.e., $R_{rs}(561)/R_{rs}(655)$, as a measure of water color. Although observations from individual bands can be sufficient to differentiate riverine plumes from seawater, band ratios increase signal-to-noise ratios and facilitate the examination of color differences (Nichol 1993b). Hereafter, we refer to the ratio of Landsat-8 bands 3 and 4 as "B3/B4" reflectance. Prior research from Apalachicola Bay (Joshi et al. 2017), a blackwater river-fed estuary along Florida's northern Gulf coast, demonstrated that an equivalent R_{rs} band ratio (i.e., $R_{rs}(551)/R_{rs}(671)$) from data collected via the Visible Infrared Imaging Radiometer Suite (VIIRS) was related to DOC through a negative power relationship, meaning that DOC absorbance is high at low values of $R_{rs}(551)/R_{rs}(671)$. This relationship can also be interpreted conversely, where DOC reflectance is low at high values of $R_{rs}(551)/R_{rs}(671)$. DOC

contributes to water color and is generally related to CDOM in estuaries receiving considerable riverine organic matter (Castillo and Carlos 2007). We thus interpret low B3/B4 reflectance values as indicative of high DOC and CDOM and, hence, freshwater.

Statistical Modeling

In addition to the visual interpretation of the reflectance values in the bands B1 to B4 and in B3/B4 mapped over the study area, five perpendicular transects of 10 km were drawn from the shoreline (distance = 0) to beyond the Great Suwannee Reef (Fig. 1) to support analysis of water color trends relative to reef locations. The transects were spaced apart by 1 km, and transect 1 (T1) was located approximately 1 km from the mouth of East Pass. All transects perpendicularly intersected the Great Suwannee Reef and also intersected Lone Cabbage Reef. We extracted R_{rs} in the individual bands B1 to B4, and the ratio B3/B4 from each pixel along the transects, which resulted in points being equally spaced every 30 m along each transect (Landsat 8 imagery has a spatial resolution of 30 m). Transect data are thus interpreted as variation in B3/B4 reflectance as a function of distance from shore. Transects were used to analyze differences in mean B3/B4 reflectance values within each of the three reef regions (i.e., from the shore to the Lone Cabbage Reef, from the Lone Cabbage Reef to the Great Suwannee Reef, and from the Great Suwannee Reef to the Gulf of Mexico).

Our primary interest in analyzing B3/B4 reflectance along transects was to determine if there were clear spatial trends in reflectance coincident with reef locations. Per our null hypothesis (i.e., reefs do not detain freshwater), B3/B4 reflectance would vary solely as a function of distance from shore (Fig. 2a). In contrast, per our study hypothesis (i.e., reefs detain freshwater), B3/B4 reflectance would vary as a function of both distance from shore and oyster reef location (Fig. 2b). To account for spatial autocorrelation, we first fit each B3/B4 transect to a spatial autoregressive model (Equation 1) that predicted B3/B4 reflectance ($\widehat{y}_{i,k}$) at a point (i) along the transect (k) as a function of lagged (x) B3/B4 reflectance in the landward direction along the transect ($y_{i\text{-}x}$); this model structure is the spatial equivalent of an autoregressive time series model.

$$\widehat{y}_{i,k} = \sum_{x=1}^{n} \beta_{i-x,k} y_{i-x,k} + \mu_k \quad (1)$$

Here, x is the lag (i.e., $x = 1$ corresponds to a spatial lag of one point in the landward direction), $\beta_{i-x,\,k}$ is the slope of the lagged term, and μ_k is the error or residuals of the model. Equation 1 thus captured the variation in B3/B4 reflectance that could be attributed to spatial autocorrelation, which we assumed occurred due to the movement of the river plume across the estuary. For each transect, autoregressive models with spatial lags of $x = \{1, 2, 3\}$ were fit in order to determine the smallest spatial lag needed to effectively remove spatial autocorrelation from the B3/B4 reflectance transects.

To determine if spatial autocorrelation was successfully removed, we applied Moran's I test to the model residuals. The null hypothesis of the Moran's I test is that of spatial independence. Once spatial autocorrelation was removed, model residuals (μ_k) were assumed to correspond to the remaining B3/B4 reflectance variance that could be attributed to effects aside from river plume discharge mixing with sea water, including that of oyster reefs. These residuals were then visually inspected to identify trends in relation to the oyster reef locations.

Results

Band reflectance

From the two images, spatial patterns in water color as quantified by B1–B4 and B3/B4 reflectance were apparent, with water-leaving reflectance for these spectra being lower in the nearshore relative to offshore (Fig. 5). In the image acquired during high river discharge (20 FEB 2015), the freshwater plume was clearly defined in water-leaving reflectance trends (Fig. 5a–e) but was less apparent during the lower flow event (Fig. 5f–j). Moreover, visual trends in reflectance appeared to coincide with the locations of the GS and LC Reefs for several bands. For example, during high freshwater discharge, B3 and B4 reflectance was markedly lower on the landward sides of both GS and LC Reefs (Fig. 6 and Fig. 5c–d), but spatial trends in B1 and B2 reflectance relative to reef locations were less evident. In contrast, during low freshwater discharge conditions, spatial trends in reflectance appeared to be associated with the reefs for B1–4 (Fig. 5f–i) but were less visually apparent for B3/B4 and B4. For both images, reflectance was higher in most bands on the seaward edges of the GS Reef and, to a lesser extent, the LC Reef (e.g., green/yellow patches in Fig. 4c,f) due to the presence of accumulated sand and sediment. The accumulated sediment is visible in the pseudo-true color versions of the images as shown in Fig. 3. The presence of accumulated sediment is not readily observable in the B3/B4 image due to the relative increase in reflectance being similar between band 3 and band 4 (Fig. 6) and, hence, being canceled out by using the band ratio. Additionally, stripes of low reflectance relative to the background and perpendicular to the GS Reef across the river plume were visible and particularly evident in the image acquired during high riverine discharge (Fig. 3b and 5a–e). These stripes may be explained by strong flows passing through gaps in the GS Reef, in turn causing turbulence that appears as stripes in water-leaving reflectance. In contrast, during lower river discharge conditions, the river plume

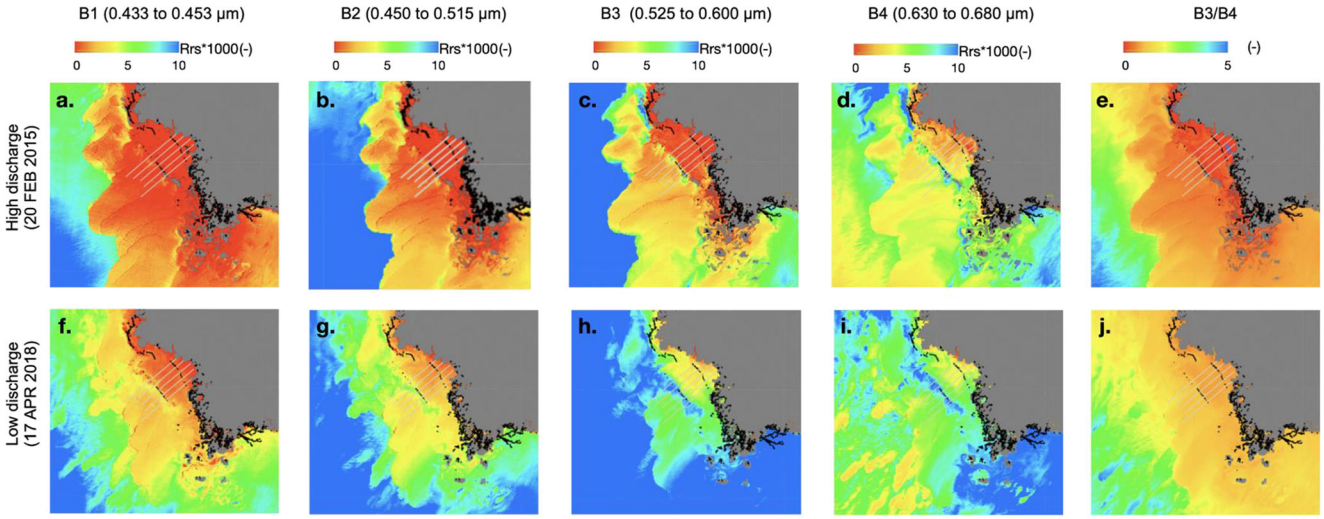

Fig. 5 Surface reflectance in bands 1–4 (B1–B4) and B3/B4 across the study area for images captured on **a**–**e** 20 of February 2015 and **f**–**j** 17 of April 2018. Land and sand features have been masked out and are shown in dark gray. Transects are indicated in light gray, and oyster reefs approximate location in black

appeared to be diverted down the LC and GS Reefs in a southeastern direction, with a large portion of the plume escaping through the gaps at the southern edges of the reef chains as indicated by a higher absorption color patch (Fig. 3c, Fig. 5g–h).

The B3/B4 reflectance values were lower and varied across a smaller range during high freshwater discharge compared to lower flow conditions (Fig. 7), indicative of the higher absorbance and, thus, greater dark river water in the estuary at high flows. Spatial trends in B3/B4 reflectance for the region

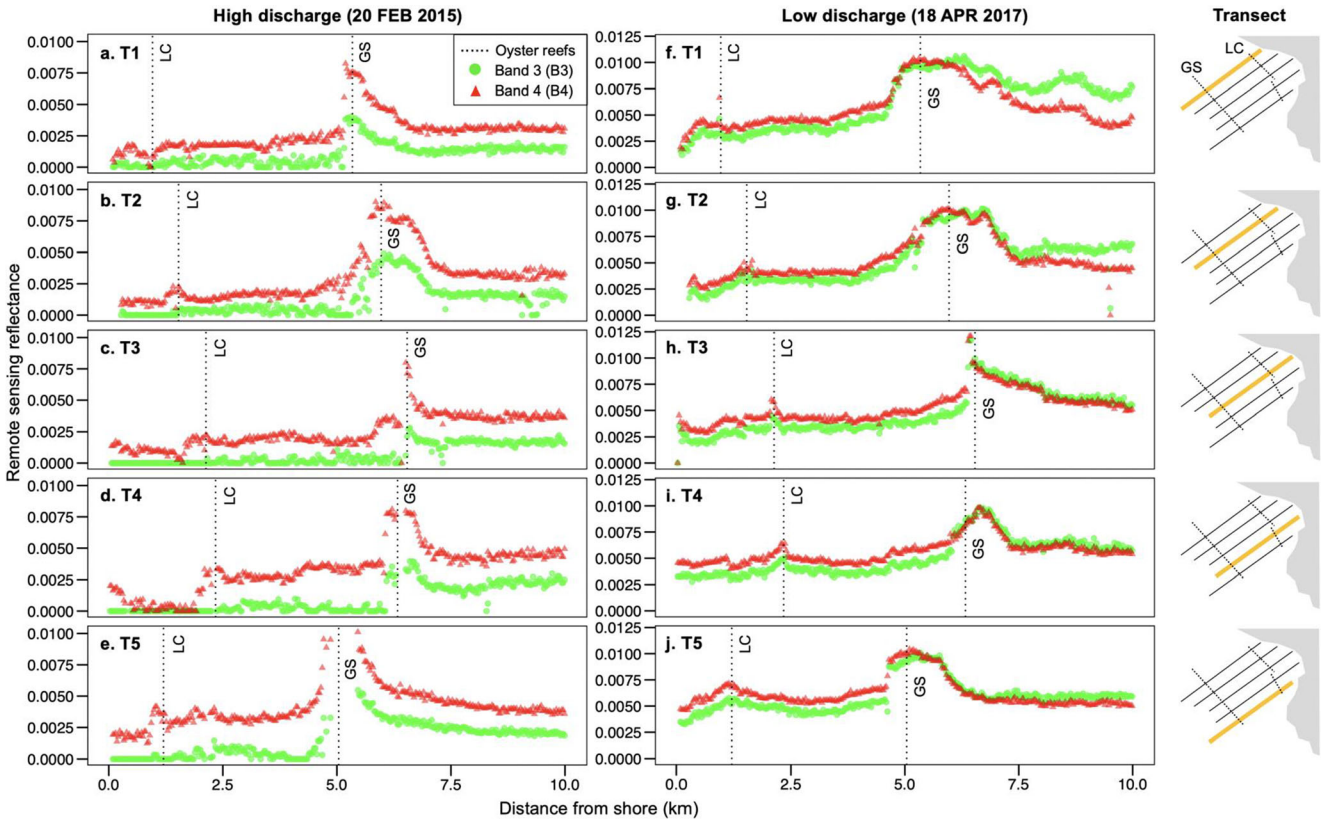

Fig. 6 Remote sensing reflectance from band 3 (B3; green circles) and band 4 (B4; red triangles) across transects 1–5 (T1–T5) when Suwannee River discharge was high (**a**–**e**) and low (**f**–**j**). Reference maps of the transects are shown to the right, with the transect corresponding to each row shown as a thick yellow line. Vertical dotted lines correspond to the locations of the Lone Cabbage (LC) and Great Suwannee (GS) Reefs

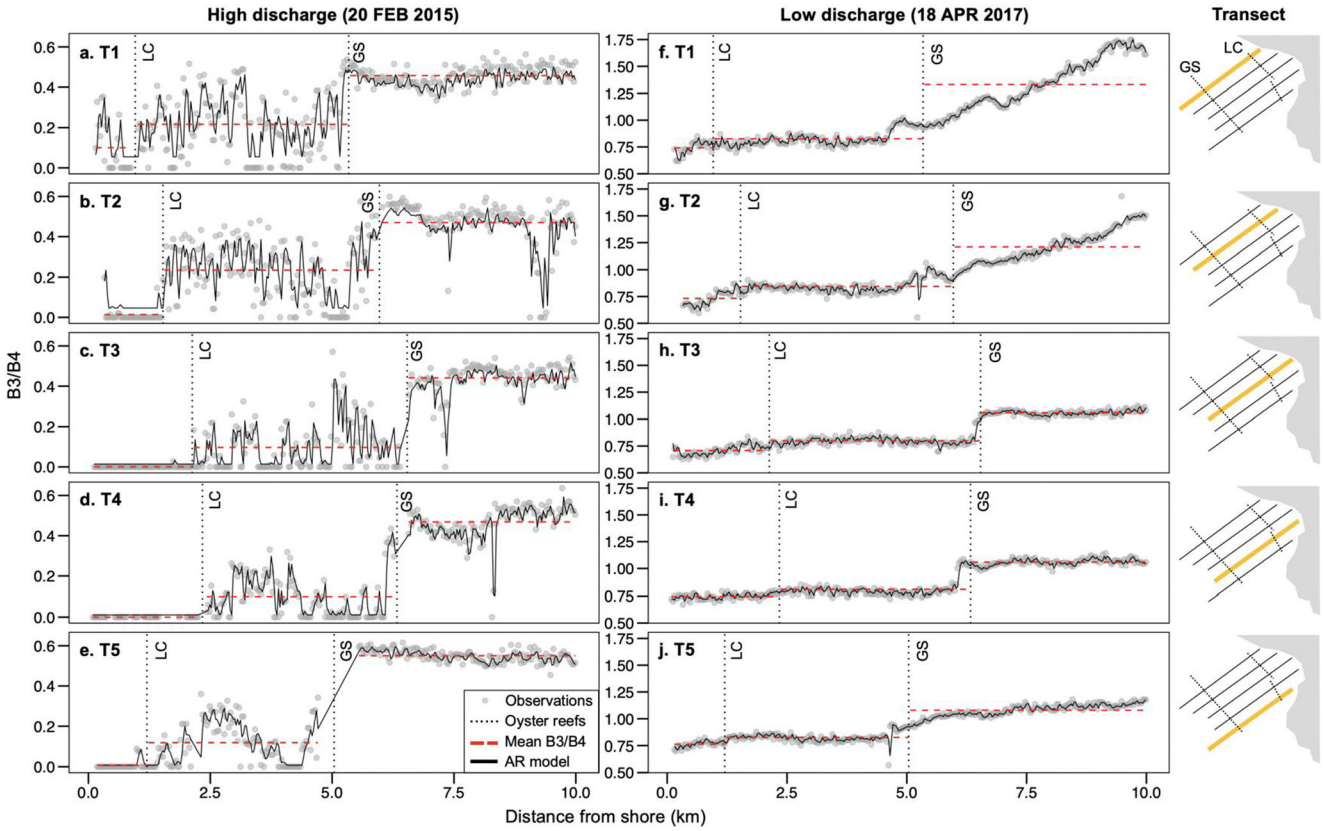

Fig. 7 Landsat-8 B3/B4 reflectance values at transects 1–5 (T1–T5) fit with spatial autoregressive models (black solid lines). B3/B4 reflectance means for the three regions are shown as dashed red lines. The Lone Cabbage (LC) and Great Suwannee (GS) Reef locations are shown as vertical dotted lines. Panels (**a**–**e**) correspond to transects extracted from the Landsat-8 image captured when freshwater discharge from the Suwannee River was high, and panels (**f**–**j**) correspond to transects extracted from the image captured under relatively low freshwater discharge conditions. Reference maps of the transects are shown to the right, with the transect corresponding to each row shown as a thick yellow line

between LC and GS Reefs were noisy and oscillatory in the high freshwater influence image but were essentially flat across this area in the lower freshwater image. Additionally, under high freshwater flow conditions, B3/B4 reflectance was near zero in the area between the shore and the LC Reef for T2 through T5 (Fig. 7b–e); the B3 and B4 reflectance patterns (Fig. 5c–d) illustrated that B3/B4 reflectance from the shore to the LC Reef was near zero because the waters in this region absorbed essentially all light in B3 (i.e., the green region of the spectrum). Relative to T2–T5, high variance was observed in B3/B4 reflectance for T1 in the region from the shore to the LC Reef, resulting in the mean B3/B4 reflectance being greater than zero on the landward side of the LC Reef for this transect. Furthermore, in the region from the LC Reef to the GS Reef, B3/B4 reflectance variance was relatively higher for T1 and T2 as compared to T3–T5, indicating that water color patterns under high flow were less consistent in the area near East Pass (i.e., where the river plume originates). The B3/B4 reflectance transects also reveal abrupt and high jumps in B3/B4 values near the location of the GS Reef, which is indicative of brighter water color. These sharp increases are particularly evident across all transects when discharge was high (Fig. 7a–d), and for T3 and T4 when discharge was low (Fig. 7h–i). During low flow, the B3/B4 values seem mostly constant until the GS Reef location, beyond which B3/B4 reflectance increases incrementally in T1 and T2, and more abruptly across T3 to T5.

Statistical Modeling of Reflectance

Spatial autoregressive models were fit to all B3/B4 reflectance transects under high and low discharge conditions (Fig. 7). Models with spatial lags of $x = \{1,2\}$ (i.e., distance = 30 m, 60 m) captured spatial autocorrelation from B3/B4 reflectance for all transects under high and low flow conditions (no significant autocorrelation in the residuals; Moran's I p value >0.05), with the exception of T5 under high flow (Table 1). Under high flow (20 FEB 2015), an autoregressive model with spatial lags of $x = \{1, 2, 3\}$ captured spatial autocorrelation from B3/B4 reflectance for T5 (no significant autocorrelation remaining in the residuals; Moran's I p value = 0.11). The residuals of the spatial autoregressive models were then examined for spatial correspondence with reef location (Fig. 8). Under low discharge conditions (Fig. 8f–j), model

Table 1 Diagnostic statistics (Moran's I and *p* value) for the residuals of spatial autocorrelation models fit with different spatial lags (*x*) to each transect (*k*) and image considered in the analysis. Low *p* values (< 0.05) indicate that spatial autocorrelation remains within the residuals

		High discharge (20 FEB 2015)		Low discharge (17 APR 2018)	
k	*x*	Moran's *I*	*p* value	Moran's *I*	*p* value
1	1	−0.25	$< 10^{-3}$	−0.30	$< 10^{-3}$
	2	−0.06	0.32	−0.05	0.38
	3	−0.03	0.65	−0.02	0.81
2	1	−0.26	$< 10^{-3}$	−0.33	$< 10^{-3}$
	2	−0.09	0.13	−0.11	0.07
	3	−0.03	0.67	−0.05	0.40
3	1	−0.25	$< 10^{-3}$	−0.35	$< 10^{-3}$
	2	−0.08	0.18	−0.08	0.20
	3	−0.05	0.45	−0.03	0.72
4	1	−0.20	$< 10^{-3}$	−0.34	$< 10^{-3}$
	2	−0.03	0.64	−0.09	0.15
	3	−0.02	0.87	−0.02	0.85
5	1	−0.47	$< 10^{-3}$	−0.36	$< 10^{-3}$
	2	−0.14	0.02	−0.10	0.08
	3	−0.10	0.11	−0.06	0.34

residuals were consistent across all three reef regions (i.e., shore to LC Reef; LC Reef to GS Reef; GS Reef to Gulf), indicating that spatial autocorrelation explained the majority of the B3/B4 trends observed from the shore to the Gulf. However, under high discharge conditions (Fig. 8a–e), residual variance changed as a function of proximity to reefs; from the shore to LC Reef, residuals were largely invariant for T2–T5, highly variant from the LC Reef to the GS Reef for all transects, and minimally variant on the seaward side of the GS Reef for all transects. For T1 under high flow conditions, variance in the residuals was high from the shore until the GS Reef. These spatial trends under high flow conditions indicate that spatial variation in B3/B4 reflectance observed across the estuary was due not only to spatial autocorrelation, but also to the oyster reef positions.

Discussion

We evaluated spatial patterns in water color from Landsat-8 images captured under hydrologically distinct conditions to infer the effect of oyster reefs on freshwater detention at the ecosystem scale of the estuary. In addition to evaluating spatial patterns by visual inspection, we also isolated the effects of spatial autocorrelation in spatial water-leaving reflectance patterns to determine if variation in reflectance could be attributed to oyster reef locations. To inspect spatial trends in water-leaving reflectance, we analyzed five 10-km transects that started at the shoreline, intersected two shore-parallel oyster reef chains—the Lone Cabbage (LC) and Great Suwannee (GS) Reefs—and terminated in marine waters of the Gulf of Mexico. Our results demonstrate that oyster reef complexes are capable of at least some level of freshwater detention under high freshwater discharge conditions, which could impact oceanographic circulation at the estuary scale. The strongest evidence of reef-driven freshwater detention was observed in the area between the shore and the LC Reef when large volumes of riverine flows were entering the estuary, while spatial patterns in water color observed during periods of low riverine discharge did not provide strong evidence of reefs affecting freshwater dispersion.

Spatial Patterns in Water-leaving Reflectance

Under high freshwater discharge conditions, spatial variation in B1–4 and B3/B4 water-leaving reflectance revealed conspicuous patterns in water color in relation to LC and GS Reefs that were consistent with our conceptual model of how B3/B4 reflectance values would vary under the scenario in which reef chains detain freshwater (Fig. 2c). In particular, when river discharge was high, the zero or near-zero B3/B4 reflectance observed in the area from the shore (i.e., distance = 0) to the LC Reef chain indicates that fresh blackwaters were pooling on the landward side of the LC Reef. Moreover, the increase in reflectance at the location of the LC Reef chain (particularly evident for T2–4, Fig. 7b–d) signals that a discontinuity in water color occurred across the LC Reef chain, which we expected to see if reef chains were detaining freshwater (Fig. 2c). The near-zero reflectance on the landward side of the LC Reef chain, which we interpret as evidence of oyster-driven freshwater accumulation, was unsurprising given this area's proximity to the primary point of discharge from the Suwannee River. The Suwannee River splits into two distributaries (Fig. 1), with the majority of flow discharging to the coast from the East Pass near the northern end of the LC Reef. The LC Reef is oriented such that it may divert flows from East Pass in a southeastern direction, potentially resulting in an accumulation of freshwater on the landward side of the LC Reef (Kaplan et al. 2016). Kaplan et al. (2016) observed a mean daily salinity differential of 3.5 ± 2.6 g/kg across the landward and seaward sides of the LC Reef in the area near the East Pass outlet, while they observed a mean daily salinity differential of only 0.1 ± 1.6 g/kg at the southeastern end of the reef nearly 5 km from East Pass. Although these prior findings indicate less of a freshwater detention effect was discernable at the southeastern end of the reef, the reflectance patterns we observed in the image acquired during high flow conditions indicated that the detention effect was more uniform along the entire landward side of the LC Reef than what was observed in the Kaplan et al.

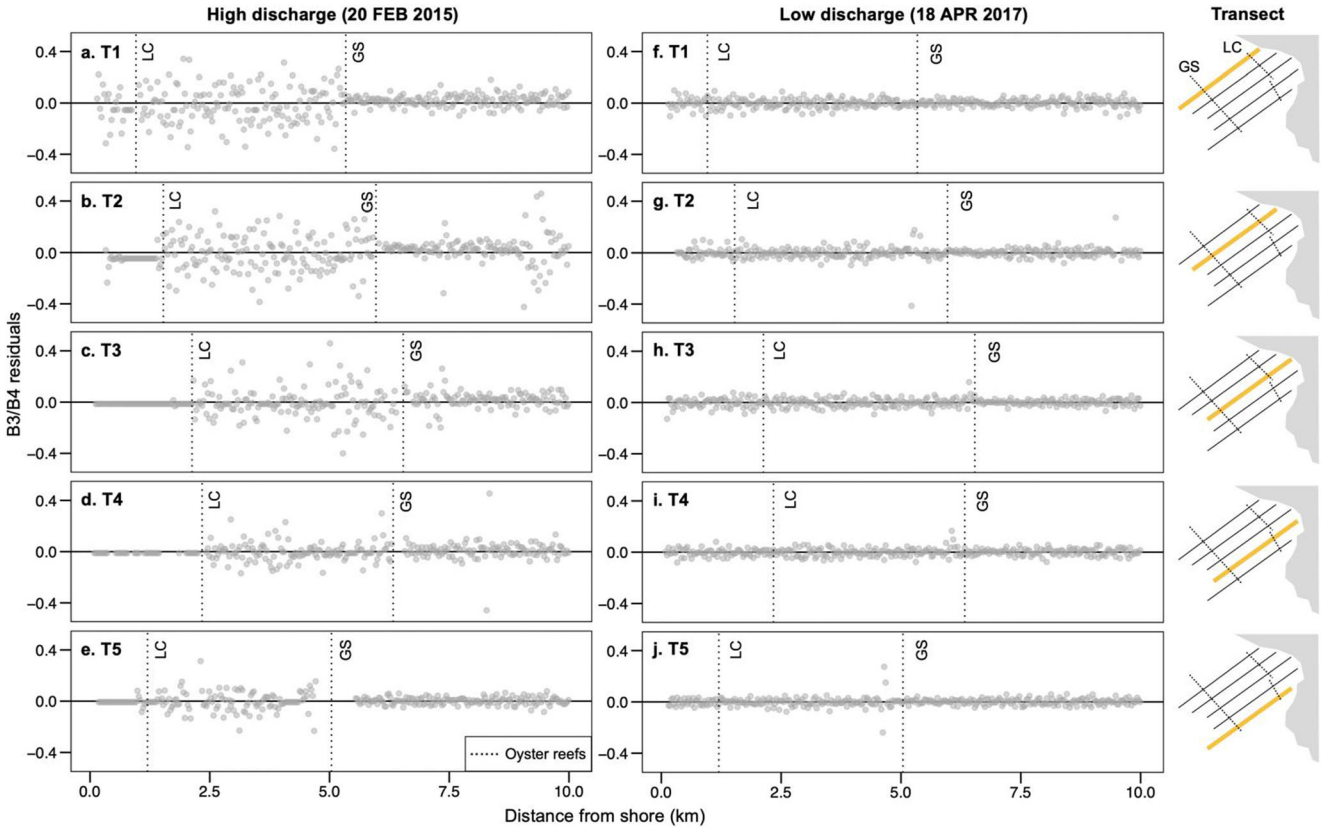

Fig. 8 Residuals from the spatial autocorrelation models for transects 1 to 5 (T1–T5). The Lone Cabbage (LC) and Great Suwannee (GS) Reef locations are shown as vertical dotted lines. Panels (**a**–**e**) correspond to transects extracted from the Landsat-8 image captured when freshwater discharge from the Suwannee River was high, and panels (**f**–**j**) correspond to transects extracted from the image captured under relatively low freshwater discharge conditions. Reference maps of the transects are shown to the right, with the transect corresponding to each row shown as a thick yellow line

(2016) study. However, the satellite images we analyzed only provided a snapshot in time, whereas Kaplan et al. (2016) collected in situ salinity measurements every 15-min for over a year. Furthermore, high flow conditions did not occur during the period monitored by the Kaplan et al. (2016) study. Thus, the conditions we observed were on the high end of the flow range for the Suwannee River, but highlight the capacity for the reef to influence freshwater detention beyond the area near the East Pass outlet when riverine inputs are high.

Furthermore, under high freshwater flow conditions, the B3/B4 reflectance values had distinct patterns across the three sections of the estuary (shore to LC Reef, LC to GS Reef, and GS Reef to the Gulf of Mexico) (Fig. 7a–e), which were also evident in the residuals of the spatial autoregressive models (Fig. 8a–e). With the exception of T1, B3/B4 reflectance was largely invariant and approximately equal to zero from the shore to the LC Reef chain, highly variable from the LC to GS Reef chains with means of approximately 0.1 to 0.2, and minimally variable on the seaward side of the GS Reef with means above 0.4. Collectively, these results support our hypothesis that oyster reefs detain freshwater at the entire estuary scale (i.e., Fig. 2c), but only when freshwater discharge is high. In contrast, when freshwater discharge was low, the variation in B3/B4 reflectance across the transects was largely explained by spatial autocorrelation, as evidenced by the residuals of the spatial autoregressive models (Fig. 8f–j). Thus, the results from low freshwater discharge conditions do not support our hypothesis.

The high variability observed in B3/B4 reflectance in the region from the LC Reef to the GS Reef during high riverine discharge might be explained by local circulation patterns, which could also explain why much less variability was observed in B3/B4 reflectance in the image acquired when riverine discharge was low. Simplified numerical modeling simulations of salinity in the Suwannee Sound demonstrated that tidal currents are stronger within gaps in the reef structures, which drives local variation in circulation patterns (Kaplan et al. 2016). Similarly, when river discharge is high, we would expect strong flows through the reef openings, resulting in local turbulence that could affect sediment resuspension and hence increase water-leaving reflectance. Accordingly, the high variance observed in B3/B4 reflectance may have corresponded to certain pixels being dominated by dark freshwater, whereas other pixels were dominated by blue-green marine waters and suspended sediment.

The B3/B4 reflectance values never reached zero during low discharge conditions as had occurred when river discharge was high, but this was likely due to there having not been enough freshwater to entirely saturate the color on the landward side of the LC Reef. Furthermore, B3/B4 reflectance trends for the transects observed in low river discharge conditions (Fig. 7f–j) appeared less discontinuous (i.e., large disparities were not observed between the beginnings and ends of the three reef regions) than those observed in high flow conditions (Fig. 7a–e). However, discontinuities could be observed in the transects under low discharge conditions near the location of the GS Reef chain (Fig. 7f–j), but these discontinuities were relatively small as compared to those seen under high flow conditions, and not apparent in autoregressive model residuals (Fig. 8f–j). The lack of variation in the residuals under low flow conditions across the three reef regions indicates that spatial autocorrelation explained most of the variance observed in these B3/B4 reflectance transects. These results diverge from those of Kaplan et al. (2016), who found that the LC Reef chain played a more consequential role in driving freshwater detention when riverine inputs were low, but this disparity may be attributed to the reliance of our approach on strong color contrast between fresh and marine waters. When riverine discharge is low, there is less opportunity for water color to visibly accumulate and saturate in areas where freshwater is detained. Although the transect-based analyses did not offer evidence of reef-driven freshwater detention when riverine discharge was low, patterns in water-leaving reflectance observed in the images acquired under low discharge offered clues about how the reefs may still influence local hydrodynamics. For example, from the image acquired during low riverine discharge (Fig. 3c and 5 g–h), the river plume was observed to move in a southeastern direction along the LC and GS Reef chains, indicating that the reefs may impede exchange and mixing of fresh and marine waters, and play a role in directing the movement of the river plume.

Benefits and Limitations of Using Landsat Data for Analysis of Estuarine Ecosystems

The work presented here highlights how Landsat-8 imagery can be used to explore large-scale estuarine dynamics through space and time. However, estuarine and coastal scientists must consider several key limitations associated with satellite image analyses. Landsat-8 has a relatively short time span (2013–present), and rather coarse temporal resolution (16-day) in comparison to ocean color satellite products (e.g., MERIS: 2001–2012, 2-day resolution; MODIS: 2000–present, daily resolution; OLCI: 2018–present, less than 2-day resolution; SeaWiFS: 1997-2010, daily resolution). Furthermore, many images are contaminated by extensive cloud cover, resulting in only a subset of the available images being of sufficient quality for analysis (Ju and Roy 2008). Although we only presented two images acquired when hydrodynamic conditions where adequate to test our study hypothesis, more images are available for further scrutiny. It is also worth noting that, although Landsat-8 OLI presents enhanced capabilities that make it more suitable for aquatic studies than its predecessors (Multi Spectral Scanner (MSS), Thematic Mapper (TM) and enhanced Thematic Mapper Plus (ETM+) aboard Landsat 1 to 5 and Landsat 7), images from earlier Landsat sensors date back to as early as 1972 (Wulder et al. 2019), and many studies have successfully used the historical Landsat archive to address water quality-related questions in lakes (Brezonik et al. 2005), rivers (Claire G. Griffin et al. 2011; Montanher et al. 2014; C. G. Griffin et al. 2018), and coastal systems (Zhang et al. 2014). Although the low signal-to-noise ratio of heritage Landsat instruments is not adequate for empirical algorithm development (Wulder et al. 2019), the images could potentially be used to investigate possible changes in the long-term feedback relationships between oyster reefs and freshwater detention by observing and quantifying spatial patterns in water-leaving reflectance over time. The Multispectral imager aboard the Sentinel-2A and B constellation is another high-resolution data source (spatial resolution of 10 to 60 meters, up to 5-day revisit frequency) valuable for coastal water monitoring (Vanhellemont and Ruddick 2016; N. Pahlevan et al. 2017a, 2017b). Landsat-8 and Sentinel-2 missions could be combined to increase temporal coverage, with their average revisit interval being approximately 3 days (Li and Roy 2017). As with older Landsat missions, extra care would need to be given to Sentinel-2 images due to their relatively wide bands, lower signal to noise ratios, and lack of calibration (Vanhellemont and Ruddick 2016).

Important limiting factors when working with satellite remote sensing for aquatic studies are the weak water-leaving reflectance relative to the top of atmosphere signal, and the contribution of sea floor bottom reflectance in shallow water environments. Here, we implemented the NASA standard atmospheric correction scheme (l2gen in SeaDAS) that has been shown to outperform other correction algorithms in optically deep water systems (Brun et al. 2015). However, alternative algorithms exist such as ACOLITE (Vanhellemont and Ruddick 2014; Vanhellemont and Ruddick 2016). Additionally, for this analysis, we considered bottom reflectance to be largely negligible given the high optical density of the blackwaters of the Suwannee River plume. However, contribution from the bottom in the overall reflectance signature was clearly evident and could not be ignored in certain areas. For example, the influence of light-colored sediment observed on the seaward side of the GS Reef was evident in the B3 and B4 transects (Fig. 6). The band ratio B3/B4 (Fig. 7) largely canceled out the effect of the sediment as the reflectance appeared to impact reflectance in the B3 and B4 bands in similar proportions and in the same direction (Fig. 6). Because this analysis focused on spatial patterns and not on specific in situ

concentrations of water quality constituents (e.g., CDOM, DOC, or salinity), corrections for bottom reflectance beyond the band ratio were considered unnecessary.

Conclusions

We leveraged the relationship between freshwater and water color in a blackwater river-fed estuary to evaluate the effect of two large oyster reef chains on freshwater accumulation and dispersion in an estuary. Our findings provide evidence of oyster reef-driven freshwater detention at the estuary scale under high freshwater discharge conditions as determined through analysis of water-leaving reflectance in Landsat-8 imagery. Moreover, although we did not uncover strong results demonstrating freshwater detention under low discharge conditions with a transect-based analysis, the visualization of the spatial variation in water color across the estuary indicated that oyster reef chains play a role in diverting the river plume even when freshwater inputs are relatively low. These results shed light on the large geospatial scale at which oyster reefs create biophysical feedbacks, insights on which contribute to our fundamental understanding of how oyster reefs act as ecological engineers in estuaries. Recognizing the scale at which oyster reefs influence estuarine circulation and freshwater accumulation is important not only for understanding estuarine ecosystem dynamics, but also for informing oyster reef restoration efforts. In particular, expensive reef restoration should be prioritized where ecosystem benefits are maximized, and this study exemplifies how satellite imagery can help with identifying such locations.

The Suwannee River Estuary, having served as an ideal study system because of the stark color contrast between its fresh and marine waters, provided a setting in which to visualize biophysical feedbacks that may be costly or logistically impossible to observe in other systems. Strong color contrast between a system's fresh and marine waters is needed for the assumptions inherent to the approach to be upheld. The same methodology could potentially be extended to evaluate reef-driven freshwater detention in estuaries that do not receive freshwater inputs from blackwater rivers as long as the fresh and marine waters mixing within the estuary have strong color contrast. Accordingly, the approach could be readily extended to other blackwater river–fed estuaries that mix with blue-green marine waters, such as those along the Gulf Coast of the southeastern United States, or to estuaries fed by turbid waters.

Although the study presented here has several limitations associated with uncertainties inherent to optical satellite remote sensing analysis, the public availability of satellite images enabled time- and cost-effective preliminary investigation of estuary-scale effects that would otherwise require extensive data and resources. To quantify the magnitude of the effect of oyster reefs on freshwater detention, satellite imagery should be complemented with extensive in situ salinity and water velocity monitoring at high spatiotemporal resolution. Additionally, because of the complex circulation patterns inherent to estuaries with dominant oyster reef structures, advanced hydrodynamic modeling would also likely be necessary to quantify the magnitude of the effects of oyster reefs on freshwater detention at the estuary scale. Such modeling efforts would require greater information on hydraulic properties of oyster reefs as well as bathymetric data, and could also benefit from satellite images to assess the accuracy of the model predictions based on observations of plume dispersion.

Funding This work is supported by the USDA National Institute of Food and Agriculture, Hatch project 1016068, and North Carolina State University. SY is supported by the U.S. Geological Survey, U.S. Fish and Wildlife Service, and the University of Florida Department of Wildlife Ecology and Conservation. Any use of trade, firm, or product names is for descriptive purposes only and does not imply endorsement by the US Government.

References

Baith, K., R. Lindasay, G. Fu, and C.R. McClain. 2001. SeaDAS, a data analysis system for ocean-color satellite sensors. *Eos Transactions AGU* 82 (202): 18.

Bales, Jerad D., Stewart A. Tomlinson, and Gina Tillis. 2006. *Flow and salt transport in the Suwannee River Estuary, Florida, 1999-2000: analysis of data and three-dimensional simulations*. *US Geological Survey Professional Paper*. https://doi.org/10.3133/pp1656b.

Beck, Michael W., Robert D. Brumbaugh, Laura Airoldi, Alvar Carranza, Loren D. Coen, Christine Crawford, Omar Defeo, Graham J. Edgar, Boze Hancock, Matthew C. Kay, Hunter S. Lenihan, Mark W. Luckenbach, Caitlyn L. Toropova, Guofan Zhang, and Ximing Guo. 2011. Oyster reefs at risk and recommendations for conservation, restoration, and management. *BioScience* 61: 107–116. https://doi.org/10.1525/bio.2011.61.2.5.

Bledsoe, Erin L., and Edward J. Phlips. 2000. Relationships between phytoplankton standing crop and physical, chemical, and biological gradients in the Suwannee River and plume region, U.S.A. *Estuaries* 23: 458–473. https://doi.org/10.1007/BF02694946.

Bowers, D.G., and H.L. Brett. 2008. The relationship between CDOM and salinity in estuaries: an analytical and graphical solution. *Journal of Marine Systems* 73: 1–7. https://doi.org/10.1016/j.jmarsys.2007.07.001.

Bowling, L.C., M.S. Steane, and P.A. Tyler. 1986. The spectral distribution and attenuation of underwater irradiance in Tasmanian inland waters. *Freshwater Biology* 16: 313–335. https://doi.org/10.1111/j.1365-2427.1986.tb00974.x.

Brezonik, Patrick, Kevin D. Menken, and Marvin Bauer. 2005. Landsat-based remote sensing of lake water quality characteristics, including chlorophyll and colored dissolved organic matter (CDOM). *Lake and Reservoir Management* 21: 373–382. https://doi.org/10.1080/07438140509354442.

Brun, Philipp, Meike Vogt, Mark R. Payne, Nicolas Gruber, Colleen J. O'Brien, Erik T. Buitenhuis, Corinne Le Quéré, Karine Leblanc, and Ya-Wei Luo. 2015. Ecological niches of open ocean phytoplankton taxa. *Limnology and Oceanography* 60 (3): 1020–1038. https://doi.org/10.1002/lno.10074.

Cao, Fang, Maria Tzortziou, Chuanmin Hu, Antonio Mannino, Cédric G. Fichot, Rossana Del Vecchio, Raymond G. Najjar, and Michael Novak. 2018. Remote sensing retrievals of colored dissolved organic matter and dissolved organic carbon dynamics in North American estuaries and their margins. *Remote Sensing of Environment* 205. Elsevier: 151–165. https://doi.org/10.1016/j.rse.2017.11.014.

Carder, Kendall L., Robert G. Steward, George R. Harvey, and Peter B. Ortner. 1989. Marine humic and fulvic acids: their effects on remote sensing of ocean chlorophyll. *Limnology and Oceanography* 34: 68–81. https://doi.org/10.4319/lo.1989.34.1.0068.

Del Castillo, Carlos E. 2007. Remote sensing of organic matter in coastal waters. In *Remote Sensing of Coastal Aquatic Environments: Technologies, Techniques and Applications*, ed. Richard L. Miller, Carlos E. Del Castillo, and Brent A. McKee, 1st ed., 7:157–180. Springer.

Chaichitehrani, Nazanin, Eurico J. D'Sa, Dong S. Ko, Nan D. Walker, Christopher L. Osburn, and Robert F. Chen. 2014. Colored dissolved organic matter dynamics in the northern Gulf of Mexico from ocean color and numerical model results. *Journal of Coastal Research* 296: 800–814.

Colden, Allison M., Kelsey A. Fall, Grace M. Cartwright, and Carl T. Friedrichs. 2016. Sediment suspension and deposition across restored oyster reefs of varying orientation to flow: implications for restoration. *Estuaries and Coasts* 39. Estuaries and Coasts: 1435–1448. https://doi.org/10.1007/s12237-016-0096-y.

Colden, Allison M., Robert J. Latour, and Romuald N. Lipcius. 2017. Reef height drives threshold dynamics of restored oyster reefs. *Marine Ecology Progress Series* 582: 1–13. https://doi.org/10.3354/meps12362.

Constantin, Sorin, David Doxaran, and Stefan Constantinescu. 2016. Estimation of water turbidity and analysis of its spatio-temporal variability in the Danube River plume (Black Sea) using MODIS satellite data. *Continental Shelf Research* 112: 14–30. https://doi.org/10.1016/j.csr.2015.11.009.

Devlin, Michelle J., Caroline Petus, Eduardo da Silva, Dieter Tracey, Nicholas H. Wolff, Jane Waterhouse, and Jon Brodie. 2015. Water quality and river plume monitoring in the Great Barrier Reef: an overview of methods based on ocean colour satellite data. *Remote Sensing* 7: 12909–12941. https://doi.org/10.3390/rs71012909.

Drusch, M., U. Del Bello, S. Carlier, O. Colin, V. Fernandez, F. Gascon, B. Hoersch, et al. 2012. Sentinel-2: ESA's optical high-resolution mission for GMES operational services. *Remote Sensing of Environment* 120: 25–36. https://doi.org/10.1016/j.rse.2011.11.026.

Farrell, Mark D., John Good, David Hornsby, Anthony Janicki, Rob Mattson, and Sam Upchurch. 2005. *Technical Report, MFL Establishment for the Lower Suwannee River & Estuary, Little Fanning, Fanning, & Mannattee Springs*.

Ferrari, G.M., and M.D. Dowell. 1998. CDOM absorption characteristics with relation to fluorescence and salinity in coastal areas of the southern Baltic Sea. *Estuarine, Coastal and Shelf Science* 47: 91–105. https://doi.org/10.1006/ecss.1997.0309.

Franz, Bryan A., Sean W. Bailey, Norman Kuring, and P. Jeremy Werdell. 2015. Ocean color measurements with the Operational Land Imager on Landsat-8: implementation and evaluation in SeaDAS. *Journal of Applied Remote Sensing* 9: 96017–96070.

Frederick, Peter. 2021. Oyster reef heights in the Suwannee Sound. Unpublished data.

Gordon, Howard R. 1978. Removal of atmospheric effects from satellite imagery of the oceans. *Applied Optics* 17: 1631. https://doi.org/10.1364/ao.17.001631.

Grabowski, Jonathan H., and Charles H. Peterson. 2007. Restoring oyster reefs to recover ecosystem services. In *Ecosystem engineers: plants to protists*, ed. Kim Cuddington, James E. Byers, William G. Wilson, and Alan Hastings, 281–298. Elsevier, Inc.: Academies Press.

Grabowski, Jonathan H., Robert D. Brumbaugh, Robert F. Conrad, Andrew G. Keeler, James J. Opaluch, Charles H. Peterson, Michael F. Piehler, Sean P. Powers, and Ashley R. Smyth. 2012. Economic valuation of ecosystem services provided by oyster reefs. *BioScience* 62: 900–909. https://doi.org/10.1525/bio.2012.62.10.10.

Griffin, Claire G., Karen E. Frey, John Rogan, and Robert M. Holmes. 2011. Spatial and interannual variability of dissolved organic matter in the Kolyma River, East Siberia, observed using satellite imagery. *Journal of Geophysical Research – Biogeosciences* 116: 1–12. https://doi.org/10.1029/2010JG001634.

Griffin, C.G., J.W. McClelland, K.E. Frey, G. Fiske, and R.M. Holmes. 2018. Quantifying CDOM and DOC in major Arctic rivers during ice-free conditions using Landsat TM and ETM+ data. *Remote Sensing of Environment* 209: 395–409. https://doi.org/10.1016/j.rse.2018.02.060.

Haven, Dexter, and James Whitcomb. 1983. The origin and extent of oyster reefs in the James River, Virginia. *Journal of Shellfish Research* 3: 141–151.

Havens, K. 2015. *Climate change: effects on salinity in florida's estuaries and responses of oysters, seagrass, and other animal and plant life*. In *EDIS document #SGEF-218*. Gainesville: FL.

Hedgpeth, Joel W. 1953. An introduction to zoogeography of the northwestern Gulf of Mexico with reference to the invertebrate fauna. *Publications of the Institute of Marine Science* 3: 170–224.

Hernández, Bersoza, Robert D. Ada, Peter Frederick Brumbaugh, Raymond Grizzle, Mark W. Luckenbach, Charles H. Peterson, and Christine Angelini. 2018. Restoring the eastern oyster: how much progress has been made in 53 years? *Frontiers in Ecology and the Environment* 16: 463–471. https://doi.org/10.1002/fee.1935.

Jordan-Cooley, William C., Romuald N. Lipcius, Leah B. Shaw, Jian Shen, and Junping Shi. 2011. Bistability in a differential equation model of oyster reef height and sediment accumulation. *Journal of Theoretical Biology* 289. Elsevier: 1–11. https://doi.org/10.1016/j.jtbi.2011.08.013.

Joshi, Ishan D., Eurico J. D'Sa, Christopher L. Osburn, Thomas S. Bianchi, Dong S. Ko, Diana Oviedo-Vargas, Ana R. Arellano, and Nicholas D. Ward. 2017. Assessing chromophoric dissolved organic matter (CDOM) distribution, stocks, and fluxes in Apalachicola Bay using combined field, VIIRS ocean color, and model observations. *Remote Sensing of Environment* 191. The Authors: 359–372. https://doi.org/10.1016/j.rse.2017.01.039.

Ju, Junchang, and David P. Roy. 2008. The availability of cloud-free Landsat ETM+ data over the conterminous United States and globally. *Remote Sensing of Environment* 112: 1196–1211. https://doi.org/10.1016/j.rse.2007.08.011.

Kaplan, David, Maitane Olabarrieta, P. Frederick, and Arnoldo Valle-Levinson. 2016. Freshwater detention by oyster reefs: quantifying a keystone ecosystem service. *PLoS One*: 1–12. https://doi.org/10.1371/journal.pone.0167694.

Katz, Brian G., Rodney S. DeHan, Joshua J. Hirten, and John S. Catches. 1997. Interactions between ground water and surface water in the Suwannee River basin. *Florida. Journal of the American Water Resources Association* 33: 1237–1254.

Kennedy, Victor S., and Lawrence P. Sanford. 1999. The Morphology and physical oceanography of unexploited oyster reefs in North America. In Oyster reef habitat restoration: a synopsis and synthesis of approaches, proceedings from the symposium, ed. M. W. Luckenbach, Roger Mann, and J. A. Wesson, 25–46. Williamsburg, VA: Virginia Institute of Marine Science, College of William and Mary. 10.21220/V5NK51.

Kutser, Tiit, Birgot Paavel, Charles Verpoorter, Martin Ligi, Tuuli Soomets, Kaire Toming, and Gema Casal. 2016. Remote sensing of black lakes and using 810 nm reflectance peak for retrieving water quality parameters of optically complex waters. *Remote Sensing* 8. https://doi.org/10.3390/rs8060497.

Le, Chengfeng, John C. Lehrter, Chuanmin Hu, and Daniel R. Obenour. 2016. Satellite-based empirical models linking river plume dynamics with hypoxic area and volume. *Geophysical Research Letters* 43: 2693–2699. https://doi.org/10.1002/2015GL067521.

Lenihan, Hunter S. 1999. Physical – biological coupling on oyster reefs: how habitat structure influences individual performance. *Ecological Monographs* 69: 251–275. https://doi.org/10.1890/0012-9615(1999)069[0251:PBCOOR]2.0.CO;2.

Li, Jian, and David P. Roy. 2017. A global analysis of Sentinel-2a, Sentinel-2b and Landsat-8 data revisit intervals and implications for terrestrial monitoring. *Remote Sensing* 9. https://doi.org/10.3390/rs9090902.

Lowe, Michael R., Troy Sehlinger, Thomas M. Soniat, and Megan K. La Peyre. 2017. Interactive effects of water temperature and salinity on growth and mortality of eastern oysters, *Crassostrea virginica*: a meta-analysis using 40 years of monitoring data. *Journal of Shellfish Research* 36: 683–697. https://doi.org/10.2983/035.036.0318.

Maritorena, Stéphane, André Morel, and Bernard Gentili. 1994. Diffuse reflectance of oceanic shallow waters: influence of water depth and bottom albedo. *Limnology and Oceanography* 39: 1689–1703. https://doi.org/10.4319/lo.1994.39.7.1689.

Marshall, Aguilar, Benoit Lebreton Danielle, Terence Palmer, De Kevin Santiago, and Jennifer Beseres Pollack. 2019. Salinity disturbance affects faunal community composition and organic matter on a restored. *Crassostrea virginica oyster reef. Estuarine, Coastal and Shelf Science*. Elsevier 106267. https://doi.org/10.1016/j.ecss.2019.106267.

McCormick-Ray, M. Geraldine. 1998. Oyster reefs in 1878 seascape pattern - Winslow revisited. *Estuaries* 21: 784–800. https://doi.org/10.2307/1353281.

McCormick-Ray, Jerry. 2005. Historical oyster reef connections to Chesapeake Bay - a framework for consideration. *Estuarine, Coastal and Shelf Science* 64: 119–134. https://doi.org/10.1016/j.ecss.2005.02.011.

Meyer, Judy L. 1990. A blackwater perspective on riverine ecosystems. *BioScience* 40: 643–651. https://doi.org/10.2307/1311431.

Montanher, Otávio C., Evlyn M.L.M. Novo, Cláudio C.F. Barbosa, Camilo D. Rennó, and Thiago S.F. Silva. 2014. Empirical models for estimating the suspended sediment concentration in Amazonian white water rivers using Landsat 5/TM. *International Journal of Applied Earth Observation and Geoinformation* 29. Elsevier B.V.: 67–77. https://doi.org/10.1016/j.jag.2014.01.001.

NASA. 2014. *Sea-viewing Wide Field-of-view Sensor (SeaWiFS) Ocean Color Data*.

NASA (n.d.). *Moderate-resolution Imaging Spectroradiometer (MODIS) Aqua Ocean Color Data*. Greenbelt, MD, USA.

Nichol, Janet E. 1993a. Remote sensing of water quality in the Singapore-Johor-Riau growth triangle. *Remote Sensing of Environment* 43: 139–148. https://doi.org/10.1016/0034-4257(93)90003-G.

Nichol, Janet E. 1993b. Remote sensing of tropical blackwater rivers: a method for environmental water quality analysis. *Applied Geography* 13: 153–168. https://doi.org/10.1016/0143-6228(93)90056-7.

NOAA Fisheries Eastern Oyster Biological Review Team. 2007. *Status Review of the Eastern Oyster (Crassostrea virginica). Northeast Regional Office*: *Report to the National Marine Fisheries Service*.

Paavel, Birgot, Helgi Arst, Liisa Metsamaa, Kaire Toming, and Anu Reinart. 2011. Optical investigations of CDOM-rich coastal waters in Pärnu Bay. *Estonian Journal of Earth Sciences* 60: 102–112. https://doi.org/10.3176/earth.2011.2.04.

Pahlevan, N., S. Sarkar, B.A. Franz, S.V. Balasubramanian, and J. He. 2017a. Sentinel-2 MultiSpectral Instrument (MSI) data processing for aquatic science applications: demonstrations and validations. *Remote Sensing of Environment* 201: 47–56. https://doi.org/10.1016/j.rse.2017.08.033.

Pahlevan, Nima, John R. Schott, Bryan A. Franz, Giuseppe Zibordi, Brian Markham, Sean Bailey, Crystal B. Schaaf, Michael Ondrusek, Steven Greb, and Christopher M. Strait. 2017b. Landsat 8 remote sensing reflectance (Rrs) products: evaluations, intercomparisons, and enhancements. *Remote Sensing of Environment* 190: 289–301.

Petes, Laura E., Alicia J. Brown, and Carley R. Knight. 2012. Impacts of upstream drought and water withdrawals on the health and survival of downstream estuarine oyster populations. *Ecology and Evolution* 2: 1712–1724. https://doi.org/10.1002/ece3.291.

Rietkerk, Max, and Johan van de Koppel. 2008. Regular pattern formation in real ecosystems. *Trends in Ecology & Evolution* 23: 169–175. https://doi.org/10.1016/j.tree.2007.10.013.

Robinson, I.S. 1983. Satellite observations of ocean colour. *Phil. Trans. R. Soc. Lond. A* 309: 415–432.

Rudorff, Natalia, Conrado M. Rudorff, Milton Kampel, and Gustavo Ortiz. 2018. Remote sensing monitoring of the impact of a major mining wastewater disaster on the turbidity of the Doce River plume off the eastern Brazilian coast. *ISPRS Journal of Photogrammetry and Remote Sensing* 145. International Society for Photogrammetry and Remote Sensing, Inc. (ISPRS): 349–361. doi:https://doi.org/10.1016/j.isprsjprs.2018.02.013.

Rybovich, Molly, Megan K. La Peyre, Steven G. Hall, and Jerome F. La Peyre. 2016. Increased temperatures combined with lowered salinities differentially impact oyster size class growth and mortality. *Journal of Shellfish Research* 35: 101–113. https://doi.org/10.2983/035.035.0112.

Scyphers, Steven B., Sean P. Powers, Kenneth L. Heck, and Dorothy Byron. 2011. Oyster reefs as natural breakwaters mitigate shoreline loss and facilitate fisheries. *PLoS One* 6. https://doi.org/10.1371/journal.pone.0022396.

Seavey, J.R., W.E. Pine, P. Frederick, L. Sturmer, and M. Berrigan. 2011. Decadal changes in oyster reefs in the Big Bend of Florida's Gulf Coast. *Ecosphere* 2: 114. https://doi.org/10.1890/ES11-00205.1.

Tehrani, Chaichi, Eurico J. D'Sa Nazanin, Christopher L. Osburn, Thomas S. Bianchi, and Blake A. Schaeffer. 2013. Chromophoric dissolved organic matter and dissolved organic carbon from sea-viewing wide field-of-view sensor (SeaWiFS), Moderatore Resolution Imaging Spectroradiometer (MODIS) and MERIS sensors: case study for the northern Gulf of Mexico. *Remote Sensing* 5: 1439–1464. https://doi.org/10.3390/rs5031439.

van de Koppel, Johan, Max Rietkerk, Norbert Dankers, and Peter M.J. Herman. 2005. Scale-dependent feedback and regular spatial patterns in young mussel beds. *The American Naturalist* 165: 66–77. https://doi.org/10.1086/428362.

van de Koppel, Johan, Tjeerd J. Bouma, and Peter M.J. Herman. 2012. The influence of local-and landscape-scale processes on spatial self-organization in estuarine ecosystems. *Journal of Experimental Biology* 215: 962–967. https://doi.org/10.1242/jeb.060467.

Vanhellemont, Quinten, and Kevin Ruddick. 2014. Turbid wakes associated with offshore wind turbines observed with Landsat 8. *Remote Sensing of Environment* 145. The Authors: 105–115. https://doi.org/10.1016/j.rse.2014.01.009.

Vanhellemont, Quinten, and Kevin Ruddick. 2016. Acolite for Sentinel-2: aquatic applications of MSI imagery. *European Space Agency, (Special Publication) ESA SP* SP-740: 9–13.

Vasilkov, A.P., V.I. Burenkov, and K.G. Ruddick. 1999. The spectral reflectance and transparency of river plume waters. *International Journal of Remote Sensing* 20: 2497–2508. https://doi.org/10.1080/014311699211895.

Walles, Brenda, João Salvador de Paiva, Bram C. van Prooijen, Tom Ysebaert, and Aad C. Smaal. 2015. The ecosystem engineer *Crassostrea gigas* affects tidal flat morphology beyond the boundary of their reef structures. *Estuaries and Coasts* 38: 941–950. https://doi.org/10.1007/s12237-014-9860-z.

Warren, M.A., S.G.H. Simis, V. Martinez-Vicente, K. Poser, M. Bresciani, K. Alikas, E. Spyrakos, C. Giardino, and A. Ansper. 2019. Assessment of atmospheric correction algorithms for the Sentinel-2A MultiSpectral Imager over coastal and inland waters. *Remote Sensing of Environment* 225. Elsevier: 267–289. https://doi.org/10.1016/j.rse.2019.03.018.

Wei, Jianwei, Zhongping Lee, Rodrigo Garcia, Laura Zoffoli, Roy A. Armstrong, Zhehai Shang, Patrick Sheldon, and Robert F. Chen. 2018. An assessment of Landsat-8 atmospheric correction schemes and remote sensing reflectance products in coral reefs and coastal turbid waters. *Remote Sensing of Environment* 215: 18–32. https://doi.org/10.1016/j.rse.2018.05.033.

Wulder, Michael A., Thomas R. Loveland, David P. Roy, Christopher J. Crawford, Jeffrey G. Masek, Curtis E. Woodcock, and Richard G. Allen, et al. 2019. Current status of Landsat program, science, and applications. *Remote Sensing of Environment* 225: 127–147. https://doi.org/10.1016/j.rse.2019.02.015.

Ysebaert, Tom, Miron Hart, and Peter M.J. Herman. 2009. Impacts of bottom and suspended cultures of mussels *Mytilus* spp. on the surrounding sedimentary environment and macrobenthic biodiversity. *Helgoland Marine Research* 63: 59–74. https://doi.org/10.1007/s10152-008-0136-5.

Zhang, Minwei, Qing Dong, Tingwei Cui, Cunjin Xue, and Songli Zhang. 2014. Suspended sediment monitoring and assessment for Yellow River estuary from Landsat TM and ETM+ imagery. *Remote Sensing of Environment* 146. Elsevier Inc.: 136–147. https://doi.org/10.1016/j.rse.2013.09.033.

Zhao, Jun, Brian Barnes, Nelson Melo, David English, Brian Lapointe, Frank Muller-Karger, Blake Schaeffer, and Hu. Chuanmin. 2013. Assessment of satellite-derived diffuse attenuation coefficients and euphotic depths in south Florida coastal waters. *Remote Sensing of Environment* 131. Elsevier Inc.: 38–50. https://doi.org/10.1016/j.rse.2012.12.009.